A Multi-Atlas Segmentation Algorithm with An Improved Sparse Representation on Brain MR Images

Hong Shi[1], Leiyi Gao[2], Ruixin Zhang[2], Junzhu Wang[2], Hongxia Deng[2]*

[1] College of artificial intelligence, Shenzhen Polytechnic, China
[2] School of computer science and technology, Taiyuan University of Technology, China
shh51@sina.com, 2360778755@qq.com, 2285575347@qq.com, axiu2019@163.com, denghongxia@tyut.edu.cn

Abstract

Macaque brains are very close to human brains, so it's an effective way to deepen the understanding of human brain functions by studying macaque brain structures. In order to segment subcortical nuclei of macaque brains more accurately, a multi-atlas segmentation algorithm based on an improved sparse representation has been designed in this paper. Firstly, a type of labeling information for atlas brain images is introduced when sparse patch-based representation is constructed, and then mutual information is improved by changing the calculation method of the information entropy, and it is used to measure the similarity between the target image and the atlas images. These two make the weights of the atlas more reasonable during fusion. Secondly, in order to fuse the segmentation results from two methods, nonlocal-patch-weighted method and the sparse representation method, a new similarity index based on a combination of dice coefficient and cosine distance is proposed. Finally, the experimental results show that this algorithm proposed in this paper has improved the accuracy of segmentation of hippocampus, striatum, claustrum and other nuclei, and it has better robustness.

Keywords: Image segmentation, MRI, Macaque, Multi-atlas, Label fusion

1 Introduction

Human brain, the major holder of high-level intelligence, one of the most complex organs in our body, seating at the highest level of our neural system, has continually been in the spotlight among scientific research frontiers. Due to moral limits, some of the brain research and experiments cannot be carried out on humans' body. Alternatively, relevant studies have shown that the brain structures of macaques (non-human primates with high intelligence) and humans are significantly similar [1]. Macaque brains possess great intelligence and a visual system highly similar to humans'. Therefore macaque brains represent the best invasive model to examine and verify hypotheses of human brain research [2]. Studying on macaque brains helps researchers reveal the principles of neuro information processing across different brain regions, through multiple levels and with simultaneous handlings. Meanwhile, the research has an important guiding significance for constructing and perfecting computing models of artificial intelligence. For all the reasons above, the research of macaque brains is growing more popular in recent years [3-4].

Analyzing MR brain images is extremely important for brain research. The analyzing procedure generally includes segmentation of different brain regions such as cerebral cortex, gray matter, white matter, cerebrospinal fluid, subcortical nuclei and so on. The crucial part of the procedure is always located at the accuracy and robustness of segmentation algorithms. First, the segmentation tools commonly used (such as FSL) are designed for analyzing human brains, not for macaque brains. So the segmentation results need to be manually adjusted and corrected by researchers. Second, due to the complexity of the spatial structures and patterns of some subcutaneous tissues such as hippocampus or lenticular nucleus, it usually requires highly-trained professionals to correct segmentation results. Third, the fuzziness of subtle structure boundaries poses a certain challenge to the segmentation algorithms. Overall, all these conditions above have caused a bottleneck to the research efficiency, so it is necessary to achieve a reliable and automatic segmentation algorithm specifically for macaque brain research.

The automatic segmentation framework released by Martin Styner et al. [5]. The steps of this framework are to first train the target region's map from the existing data set, and then segment it through the map. In 2017, Balbastrey [6] improved Gaussian Mixture Model (GMM) method and released a segmentation tool for macaques. It was integrated into BrainVISA version 4.6 as a component and applied to segment T2 images of macaque brains. The shortage of the tool is that the number of brain tissues it can mark up at one time is limited.

Compared with Balbastrey's method, multi-atlas image segmentation methods can introduce more priori information to improve accuracy. Therefore many researchers focus on multi-atlas segmentation methods. Some of the researchers have published various MRI templates, MR images and data sets of rhesus monkeys [7-9]. M. P. Milham et al. [10] compared the existing public datasets of non-human primates. Weidao Chen et al. [11] used multi-atlas segmentation to identify macaque brain tissues. Recently, with the rapid development of AI, deep learning methods have also applied to MR image segmentation algorithms. Huo et al. [12] used 3D-UNET to segment human brains. Zhao et al. [13] used

*Corresponding Author: Hongxia Deng; E-mail: denghongxia@tyut.edu.cn
DOI: 10.53106/160792642023112406019

deep learning methods to extract useful information of on-human primate brains. However, for accurate segmentation of macaque brains, multi-atlas methods need a large amount of training data, but the current macaque datasets are not sufficient. So, as of today, instead of using multi-atlas, most researchers use single-atlas to segment macaque brains, but they desire more datasets and more reliable multi-atlas tools.

In the field of human brain multi-atlas segmentation, Zhang et al. [14] introduced the sparse representation algorithm into multi-atlas label fusion, and achieved excellent results. Another paper proposed by Meng Yan et al. [15-16] has also contributed the sparse representation by using label fusion method. Rui Xia et al. [17] proposed an improved multi-atlas image segmentation algorithm based on resampling. Liu et al. [18] proposed an effective segmentation method based on atlas registration and linearization, but running this algorithm consumes a lot of time.

Julia A. Scott [19] et al. obtained the required segmentation results by registering macaque data into the existing atlas, and then manually modifying it. S. Gouttard [20] and others trained the atlas with spatial probability prior by using the manually marked training set, successively registered the atlas image to the target image to obtain the deformation field, applied the deformation field to the corresponding atlas probability map, and took 0.5 as the threshold to segment the lateral ventricle, hippocampus, putamen, caudate nucleus, globus pallidus and amygdala. R. Wolz [21] combined the multiple map segmentation method and the map cutting method to construct the probability map of the specific region of interest, without relying on the manually labeled training set, and divided six pairs of subcortical nuclei. Wu et al. [22] proposed clustering the atlases after common registration, thus providing an effective strategy to find the most similar example atlases to improve the accuracy of segmentation.

To sum up, after studying the currently existing methods of MRI segmentation, this paper chose the way of segmentation based on multi-atlas images with the sparse representation algorithm for in-depth research. By elaborate analyses, we found that the common algorithm contains insufficient information during the fusion process, and it only considers the voxels related to target image voxels, and it lacks global similarity measurement. Moreover, sparse representation also loses some information of image patches, which will lead to segmentation errors. So an improved multi-atlas segmentation label fusion algorithm based on an improved sparse representation (ISRLF) is proposed here. This algorithm introduces mutual information by changing the calculation method of information entropy, and then adjusts the weight of each atlas image during fusion process to make it more reliable, so as to improve the accuracy for macaque brain segmentation. Besides, the algorithm also proposes a similarity index, which synthesizes the results of the weighted fusion algorithm of nonlocal patches and the results of sparse representation, and overcomes the shortcoming that sparse representation will lose information to some extent. The similarity index includes an improved L-Dice coefficient and cosine distance, and finally achieves better segmentation results.

2 Background Description

Sparse representation was originally applied in the field of signal processing. Its idea is to replace the original signal with a combination of some basic signal marks, so that to reduce the amount of processing data as much as possible. As shown in formula (1) blow, T is the represented signal and D is the dictionary matrix, α is the sparse coefficient. Sparse representation has been applied to image compression, super-resolution reconstruction and feature extraction in the field of image processing. Sparse coefficient α is obtained by formula (2), Where x is the original signal to be represented.

$$T = D\alpha \,. \tag{1}$$

$$\hat{\alpha} = \underset{\alpha}{\operatorname{argmin}} \left\| x - D\alpha \right\|_2^2 + \lambda \left\| \alpha \right\|_1 . \tag{2}$$

3 ISRLF Method

3.1 Methodology Framework

In this paper, the segmentation method of multi-atlas sparse representation has been improved, and a new label fusion algorithm combining sparse representation fusion method and nonlocal-patch-weighted method is proposed to segment the subcortical nuclei of macaque monkey brains. Figure 1 is a frame diagram of the new method.

The algorithm steps are as follows:

(1) Obtain linearly registered images Li by linear registration calculating on atlas gray images.
(2) Obtain non-linearly registered images Fi by non-linear registration calculating. Then register atlas label images to target image to obtain registered images Ii.
(3) Obtain pre-segmentation results by locally weighted fusion method on target image.
(4) Create target label patches Tpx and atlas label patches Tpi. All the atlas label patches (cdi) form a complete dictionary D, that is, D = [Tp1, Tpi , Tpn]], for sparse representation.
(5) Introduce mutual information, improve the calculation algorithm of information entropy, measure the global similarity of the corresponding atlas planes after linear registration, calculate the average value, and improve sparse representation to calculate weights.
(6) Two fusion methods, sparse representation label fusion and nonlocal-patch-weighted label fusion, are both used to segment the target image, and obtain two fusion results (not the final result).
(7) The combination of Dice coefficient and cosine distance is used to measure the segmentation results, and the segmentation results of the two fusion methods are fused again to obtain the final segmentation result.

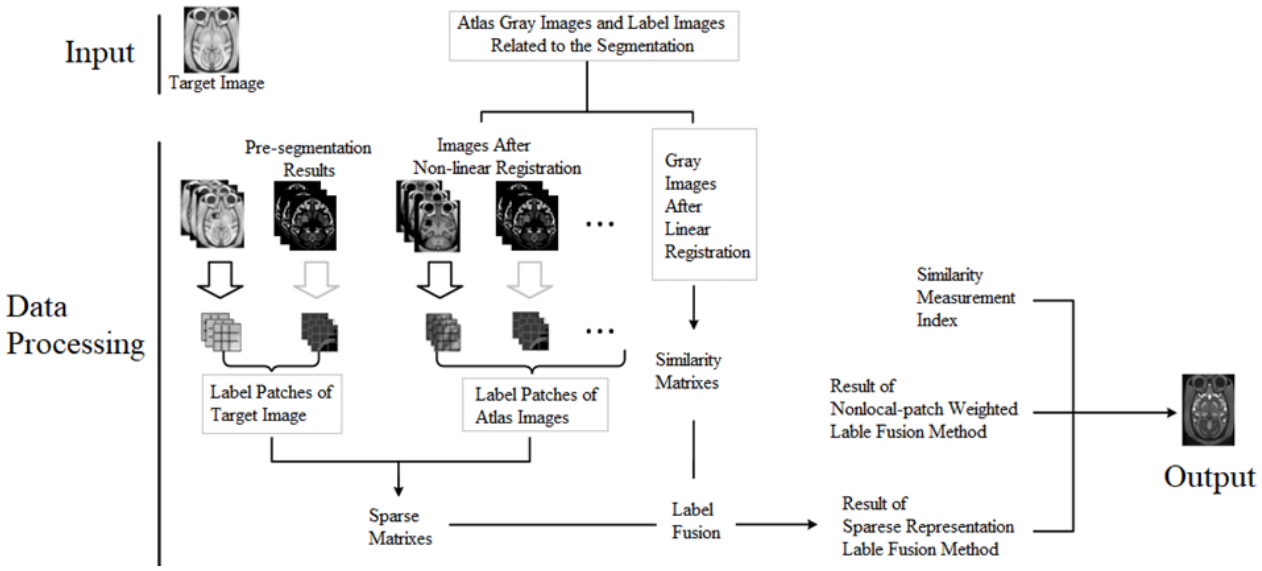

Figure 1. Method framework

3.2 The Construction of Target Image Label Patches and Atlas Image Label Patches

Among most common sparse representation methods, the information contained in image patches is just gray values, which are limited and do not make full use of priori information. In this paper, the gray information of atlas images and the label information of the label images are combined and introduced into target image as well as atlas gray images respectively, to form the target image label patches and the atlas image label patches, so as to enrich the information carried by image patches, so as to optimize the weight of each atlas image during label fusion.

In this paper, D99-SL, NMT and inia19 were used for segmentation. In order to introduce the label information in the atlas, the target image needs to be pre-segmented. This method uses a locally weighted method to pre-segment the target image. After constructing the initial image patches which only contain gray information, the corresponding label value patches are transformed into binary forms, and then combined with the initial image patches to form a new set of image label patches. The specific way of the binarization is to take the label value of a center voxel as the reference value, and then all the label values that are equal to the reference value are recorded as 1, otherwise they are recorded as 0.

The specific process of constructing the atlas image label patches is shown in Figure 2. First, taking the voxel x of the atlas gray image Fi (nonlinear registration) as the center and r×r×r as the size, construct the initial image patch adi. Second, from the nonlinear atlas image It, taking the label at the corresponding position as the center and r × r × R as the size, construct the label patch bdi and binarize it. Third, transform adi and bdi respectively into column vectors and splice them to form the atlas image label patch Tpi.

The construction process of target image label patches is similar to that of atlas image label patches. First, taking the target voxel x as the center and r × r × r as the size, construct target image patch adx. Second, taking the corresponding position x of the pre segmentation result as the center, and r × r × r as the size, construct label patch bdx. Third, transform adx and bdx into column vectors respectively, and combine them to form target image label patch Tpx.

For the target image label patches Tpx, select each label patch Tpi to form an complete dictionary D, that is, d = [Tp1, Tpi, Tpn]. Calculate the sparse matrix according to formula (2), where x is the target image label patch. And then take the calculated sparse coefficient as the initial weight matrix W1 of the atlas.

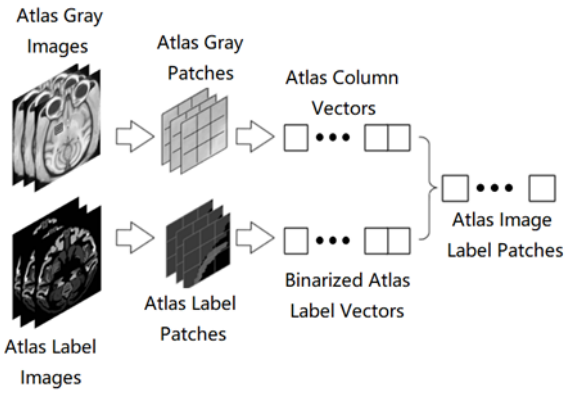

Figure 2. The construction of atlas image label patches

3.3 Image Similarity Calculation Based on Mutual Information

The sparse representation label fusion method only considers the voxels in the target image patch that is centered on the target voxel, and does not consider the similarity between the atlas images and the target image from a global perspective. So in the process of label fusion, adding a measurement of the overall image similarity is helpful to improve the segmentation effect. In information theory, there is a concept called mutual information, that is, in the field of image processing, the similarity of two images is often determined by measuring the information entropy of two

images. Therefore, this method introduces mutual information to measure the similarity of atlas gray images. Larger value of mutual information between two images means they are more similar. Formula (3) is the calculation formula of the image information entropy, in which the probability PM is obtained from formula (4). Gray level histograms are used during the calculation of formula (4), where hi represents the number of voxels whose gray value is i, and the denominator represents the total number of voxels in the image.

$$H(M) = -\sum_{M} p_M(m) \log p_M(m). \quad (3)$$

$$p_M = \frac{h_i}{\sum_{i=0}^{N-1} h_i}. \quad (4)$$

Usually, the mutual information between gray images is calculated from gray histograms, but this way has a shortcoming for NMR analysis. For example, the voxels with the gray value 0 in the MRI image represents the background of the image, and generally, those background voxels are included in the calculation for mutual information. But MRI images only focus on the brain region, so the background can be basically ignored. If there are many voxels with zero gray value and few voxels with none-zero value, the mutual information value will be very large, whereas the actually important part, the brain structures, may not be very similar. In addition, due to the limited prior information for common calculation of mutual information based on gray histograms, the similarity of the two images cannot be well measured.

In order to solve the two problems above, this method modifies the formula for calculating information entropy.

Firstly, the voxels with the gray value 0 are eliminated and not included in the probability calculation. The adapted probability pM of gray value is calculated according to formula (5).

$$p_{M'} = \frac{h_i}{\sum_{i=1}^{N-1} h_i}. \quad (5)$$

Secondly, due to the importance of brain gray matter, this method focuses on subcortical nuclei. Therefore, this method obtains the probability ratio β of the gray matter in the overall image of the brain according to formula (6), so as to achieve the purpose of measuring the voxel similarity of the brain structure. And ratio β is introduced into the information entropy calculation of gray images.

$$\beta = \frac{p(G)}{p(W) + p(G)}. \quad (6)$$

In order to increase the prior information, label images are introduced to calculate the information entropy, according to formula (7). I_M represents the label image, and m represents the number of subcortical nuclei in the image. Since Dice coefficient can represent the similarity of nuclei, it is introduced into the calculation process as a parameter to enrich the priori information. As shown in formula (8), the dice coefficient of the target image segmentation results I_A and I_B for label j are obtained, and the result introduced into the calculation of the improved information entropy as a parameter γ.

$$H(I_M) = \sum_{j=1}^{m} p(I_{M_j}) \log p(I_{M_j}). \quad (7)$$

$$\gamma = Dice(I_{A_j}, I_{B_j}). \quad (8)$$

Thus, the improved expression of information entropy is formula (9). For the given two images A and B, $H_1(A)$ and $H_1(B)$ are the information entropies, and the calculation methods are formula (10) and (11). $H_1(A,B)$ is the joint information entropy of both A and B, and its calculation is formula (12). $I_1(A,B)$ is the mutual information between A and B, and its calculation is formula (13).

$$H_1(M) = \beta H(M) + \gamma H(I_M). \quad (9)$$

$$H_1(A) = -\beta \sum_{a} p_{A'}(a) \log p_{A'}(a) + \gamma H_1(I_A). \quad (10)$$

$$H_1(B) = -\beta \sum_{a} p_{B'}(b) \log p_{B'}(b) + \gamma H_1(I_B). \quad (11)$$

$$H_1(A,B) = -\beta \sum_{a \cdot b} p_{A' \cdot B'}(a,b) \log p_{A' \cdot B'}(a,b) + \gamma H_1(I_A, I_B). \quad (12)$$

$$I_1(A,B) = H_1(A) + H_1(B) - H_1(A,B). \quad (13)$$

Take the calculated mutual information of sagittal plane, coronal plane and axial plane as matrixes Sim1, Sim2 and sim3, extract the similarity value corresponding to the target voxel (a, b, c) in the matrixes, and calculate the similarity value of voxel x according to formula (14). Then calculate the final map fusion weight according to formulas (15) and (16).

$$Sim(x) = \frac{Sim1(a) + Sim2(b) + Sim3(c)}{3}. \quad (14)$$

$$W_2 = W_1 * Sim(x). \quad (15)$$

$$W_3(i) = \frac{W_2(i) - \min}{\min - \max}. \quad (16)$$

3.4 Label Fusion

There are two image patch-based label fusion methods. One is nonlocal-patch-weighted fusion method that measures the similarity between all image patches participating in the label fusion and the patches of the target image. The other

is sparse representation method, in which it uses sparse to represent the target image patches and the atlas image patches.

Nonlocal-patch-weighted label fusion method does not discard the image patches involved in the fusion, and has more redundant information, which is an advantage. Compared with the nonlocal-patch-weighted fusion method, the sparse representation fusion method will discard some details. However, sparse representation fusion method also has an incomparable advantage that it's better to give clearer boundary points in the segmentation result.

In order to combine all the advantages of the two methods and improve the segmentation accuracy for brain subcutaneous nuclei, this method combines nonlocal-patch-weighted method with sparse representation method, and proposes a new label fusion method -- ISRLF.

The process of image patch-weighted fusion method is as follows:

(1) Each atlas gray image and label image are registered into the target image T to obtain the registered gray image F_i and label image I_i.

(2) From T, extract target image patch Tp_x which takes x as the center and r × r × r as the size (r=3 in the experiments). The extraction process is that in each atlas image, taking voxel x as the center and r × r × r as the size, search neighborhood to extract all image patches Tp_i involved in label fusion.

(3) Calculate the weight of each image patch, and then calculate the label value probability according to formula (17).

(4) Calculate label results according to formula (18).

The image patches extracted in this method are image label patches. The common nonlocal-patch-weighted method uses the normalized correlation coefficient (NCC) to measure the similarity between the target image patches and the extracted atlas image patches. The label fusion method of sparse representation is to construct the target image label patches and the atlas image label patches, take the atlas image label patches as an over complete dictionary d = [TP1, TPI, TPN], calculate the sparse coefficient according to formula (2), and then obtain the final atlas weights through formulas (14), (15) and (16). Then, the segmentation result is obtained according to formulas (17) and (18).

$$sumw(x) = \frac{\sum_{i=1}^{n} w_i l_i}{\sum_{i=1}^{n} w_i}. \tag{17}$$

$$L_T(x) = \begin{cases} 1 & sumw(x) \geq 0.5 \\ 0 & sumw(x) < 0.5 \end{cases}. \tag{18}$$

In order to fuse the two segmentation methods, a similarity measure function has been created in this paper as in formula (19). The function consists of two parts. The first part is Dice coefficient and the second part is cosine distance. In the formula, similarity value is inversely proportional to dice coefficient and directly proportional to cosine distance, R is pre segmentation result at the target voxel x, R is the pre segmentation result at voxel x, R_1 is the fusion result of nonlocal-patch-weighted method, and R_2 is the fusion result of sparse representation fusion method.

$$D_{Ri} = \mu \frac{1}{Dice(R, Ri) + d} + (1-\mu)\cos(p(x), p_i(x)) \quad i = 1, 2. \tag{19}$$

In formula (19), $Dice(R,R_i)$ is the dice coefficient of the pre segmentation result and R_1 or R_2, and d is a constant. The constant d is added to prevent the denominator from being zero. $p_i(x)$ represents the column vector transformed from an image patch that is centered on voxel x from the result of nonlocal-patch-weighted method or sparse representation method. $cos(p(x),p_i(x))$ is the cosine distance of two column vectors. μ and 1 - μ represent their weights. The greater the D_{Ri} value, the lower the similarity.

Formula (20) is the fusion formula of the two methods. When the two label values of the two segmentation methods are equal, the label value is given to voxel x. When the segmentation results of the two methods are different, the similarity value is calculated through formula (19). If $D_{R1}>D_{R2}$, it shows that the difference between R_1 and R is larger than that between R_2 and R, and the result R_2 is given to voxel x. If $D_{R1}<D_{R2}$, the result R_1 is given to voxel x.

$$L_T(x) = \begin{cases} R_1 & if(R_1 = R_2) \ or \ (D_{R1} < D_{R2}) \\ R_1 & if(D_{R1} > D_{R2}) \end{cases}. \tag{20}$$

4 Experiment and Result Analysis

4.1 Data Introduction

The test data set used in the experiment is the macaque data set published by Oxford University. The data set collected data of 20 male macaques with 3T scanner. The data set includes T1, resting fMRI, and T1 data were used in this experiment. The age distribution of rhesus monkeys is 2.41-6.72 years (average age is 4.01 years) and the weight distribution is 4.35-11.7 kg (average weight is 6.57 kg). The voxel resolution is 0.5 × 0.5 × 0.5mm, TE is 4.01ms, TR is 2500ms, TI is 1100ms, and the turnover angle is 8 °.

4.2 Evaluation Index

Dice coefficient is selected to evaluate the segmentation quality in the experiment, and its calculation method is shown in formula (21). In the formula, A represents the expert standard segmentation result (the standard gold result), |?| Represents the number of voxels in each set, |A ∩ B| represents the number of voxels with the same voxel label corresponding to set A and set B, | a | + | B | represents the number of voxels in set A and set B. The value range of Dice coefficient is 0 to 1. The closer it is to 1, the higher the accuracy.

Dice coefficient

$$Dice(A,B) = 2\frac{|A \cap B|}{|A| + |B|}. \quad \textbf{(21)}$$

4.3 Result Analysis

In this experiment, three methods were selected to compare the segmentation results of hippocampus, striatum and claustrum with the standard gold result. The methods are Majority Voting (MV), Joint Label Fusion (LW Joint), Weighted fusion algorithm (WV), Non local block based algorithm (PATCH)and the method in this paper (ISRLF).

Figure 3(a) to Figure 3(f) show the segmentation results of the five different methods respectively. Among them, Figure 3(a) is the standard gold segmentation result, Figure 3(b) is the MV segmentation result, Figure 3(c) is the LW Joint segmentation result, Figure 3(d) is the WV segmentation result, Figure 3(e) is the PATCH segmentation result and Figure 3(f) is the ISRLF segmentation result. It's clear that among these figures the LW Joint result is the worst, and the ISRLF result is the best.

Table 1 shows the segmentation accuracy of selected nuclei using the above five methods on the macaque dataset from Oxford University. Figure 4 is a box diagram of dice coefficients of segmentation results of five methods. It can be seen from Table 1 and Figure 4 that although the segmentation accuracy of MV method for hippocampus is higher than that of LW joint, the stability of this method is very poor, the accuracy fluctuates greatly, and the accuracy of hippocampus fluctuates more than 10% relative to the average value. The accuracy of LW joint method fluctuates within 10% relative to the average value, and the stability is good, but only the claustrum segmentation accuracy exceeds that of MV method. The method of this paper improves all the accuracies of the three nucleus segmentations, especially for striatum segmentation, which is about 8% higher than MV method. The improvement on claustrum segmentation is not significant, but the result fluctuates within 5%, which is much better than MV and LW joint, indicating the stability of ISRLF is the highest among the five methods. Among the four algorithms compared with this algorithm, PATCH algorithm has the best segmentation effect, followed by WV algorithm. PATCH algorithm is slightly lower than WV algorithm in the segmentation accuracy of striatum. The similarity of Dice coefficients of other nuclei has achieved the best results except this algorithm. It can be seen that the method proposed in this paper has better robustness compared with other methods.

Figure 5 is an effect diagram showing the coronal segmentation results of three nuclei separately. The first to the third rows are hippocampus, striatum and claustrum. The first to fourth columns are the gold standard, MV method segmentation result, LW joint segmentation result, Weighted fusion algorithm (WV) segmentation result. Non local block based algorithm (PATCH) segmentation result and ISRLF segmentation result respectively. It can be seen that this paper's segmentation results are better than those of other methods.

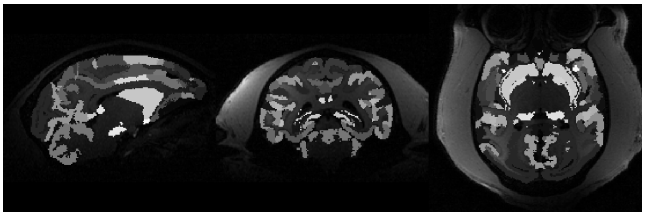

(a) Gold standard

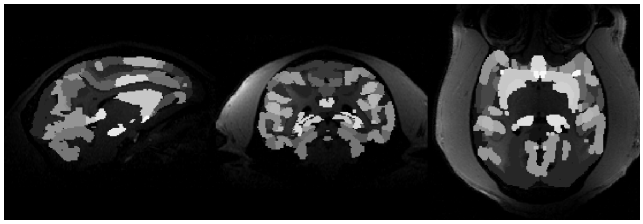

(b) MV method segmentation result

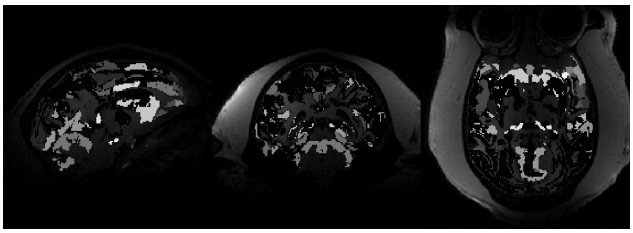

(c) LW joint segmentation result

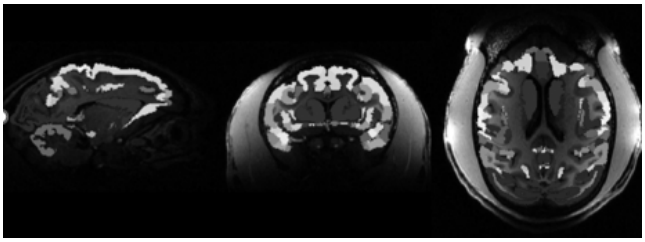

(d) WV segmentation result

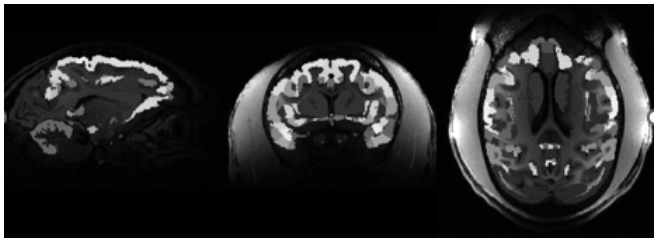

(e) PATCH segmentation result

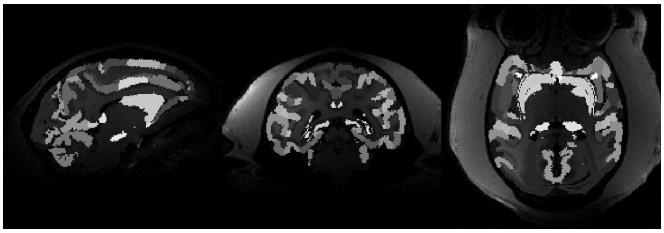

(f) ISRLF segmentation result

Figure 3. Segmentation results of three different methods

Table 1. Dice coefficient results of three methods

	MV	LW joint	ISRLF
Hippocampus	38.56%	31.18%	58.92%
Hippocampus	± 12.94%	± 9.64%	± 2.45%
Striatum	67.56%	50.46%	87.91%
Striatum	± 4.01%	± 8.54%	± 1.05%
Claustrum	33.83%	45.25%	62.43%
Banded nucleus	± 9.65%	± 5.61%	± 2.10%

	WV	PATCH	ISRLF
Hippocampus	52.00%	54.66%	58.92%
Hippocampus	± 6.55%	± 4.20%	± 2.45%
Striatum	85.61%	85.37%	87.91%
Striatum	± 1.60%	± 1.61%	± 1.05%
Claustrum	57.58%	59.03%	62.43%
Banded nucleus	± 2.98%	± 2.28%	± 2.10%

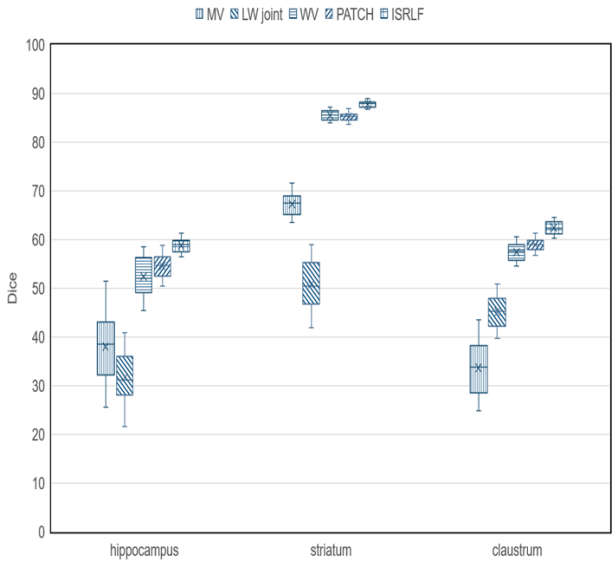

Figure 4. Dice coefficient

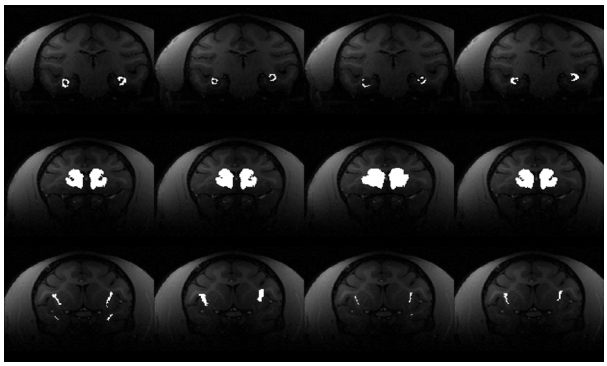

Figure 5. Cross sectional segmentation results of hippocampus, striatum and claustrum

5 Conclusion

This paper has proposed a multi-atlas brain MR image segmentation algorithm based on an improved sparse representation, and it has applied the algorithm to the segmentation of macaque brain subcutaneous nuclei. The algorithm increases the prior information of image patches, improves the mutual information by changing the calculation method of information entropy, and uses the mutual information to measure the global similarity to make the weight of each map more reasonable during fusion. Then a similarity index is proposed to synthesize the segmentation results of sparse representation label fusion method and nonlocal-patch-weighted label fusion method, so as to obtain the final segmentation result. By comparing the Dice coefficient with the results obtained by other methods, it is proved that this proposed method in this paper has higher accuracy and better robustness.

References

[1] M. M. Quallo, C. J. Price, K. Ueno, T. Asamizuya, K. Cheng, R. N. Lemon, A. Iriki, Gray and white matter changes associated with tool-use learning in macaque monkeys, *Proceedings of the National Academy of Sciences*, Vol. 106, No. 43, pp. 18379-18384, October, 2009.

[2] M. D. Bauman, C. M. Schumann, Advances in nonhuman primate models of autism: Integrating neuroscience and behavior, *Experimental neurology*, Vol. 299, pp. 252-265, January, 2018.

[3] P. Wang, D. Wang, J. Zhang, R. Bai, M. Qian, Y. Sun, Y. Lu, X. Zhang, Evaluation of Submillimeter Diffusion Imaging of the Macaque Brain Using Readout-Segmented EPI at 7 T, *IEEE Transactions on Biomedical Engineering*, Vol. 66, No. 10, pp. 2945-2951, October, 2019.

[4] M. Styner, R. Knickmeyer, S. Joshi, C. Coe, S. Short, J. Gilmore, Automatic brain segmentation in rhesus monkeys, *SPIE Medical Imaging*, Vol. 6512, pp. 883-890, March, 2007.

[5] J. T. Young, Y. Shi, M. Niethammer, M. Grauer, C. L. Coe, G. R. Lubach, B. Davis, F. Budin, R. C. Knickmeyer, A. L. Alexander, M. A. Styner, The UNC-Wisconsin rhesus macaque neurodevelopment database: A structural MRI and DTI database of early postnatal development, *Frontiers in neuroscience*, Vol. 11, Article No. 29, February, 2017.

[6] Y. Balbastre, D. Rivière, N. Souedet, C. Fischer, A. S. Hérard, S. Williams, M. E. Vandenberghe, J. Flament, R. Aron-Badin, P. Hantraye, J. F. Mangin, T. Delzescaux, Primatologist: a modular segmentation pipeline for macaque brain morphometry, *Neuroimage*, Vol. 162, pp. 306-321, November, 2017.

[7] J. Seidlitz, C. Sponheim, D. Glen, F. Q. Ye, K. S. Saleem, D. A. Leopold, L. Ungerleider, A. Messinger, A population MRI brain template and analysis tools for the macaque, *Neuroimage*, Vol. 170, pp. 121-131, April, 2018.

[8] C. Reveley, A. Gruslys, F. Q. Ye, D. Glen, J. Samaha, B. E Russ, Z. Saad, A. K Seth, D. A. Leopold, K. S. Saleem, Three-dimensional digital template atlas of the macaque brain, *Cerebral Cortex*, Vol. 27, No. 9, pp. 4463-4477, September, 2017.

[9] T. Rohlfing, C. D. Kroenke, E. V. Sullivan, M. F. Dubach, D. M. Bowden, K. A. Grant, A. Pfefferbaum, The INIA19 template and NeuroMaps atlas for primate brain image parcellation and spatial normalization, *Frontiers in neuroinformatics*, Vol. 6, Article No. 27, December, 2012.

[10] M. P. Milham, L. Ai, B. Koo, T. Xu, C. Amiez, F. Balezeau, M. G. Baxter, E. L. A. Blezer, T. Brochier, A. Chen, P. L. Croxson, C. G. Damatac, S. Dehaene, S. Everling, D. A. Fair, L. Fleysher, W. Freiwald, S. Froudist-Walsh, T. D. Griffiths, C. Guedj, F. Hadj-Bouziane, S. B. Hamed, N. Harel, B. Hiba, B. Jarraya, B. Jung, S. Kastner, P. C. Klink, S. C. Kwok, K. N. Laland, D. A. Leopold, P. Lindenfors, R. B. Mars, R. S. Menon, A. Messinger, M. Meunier, K. Mok, J. H. Morrison, J. Nacef, J. Nagy, M. O. Rios, C. I. Petkov, M. Pinsk, C. Poirier, E. Procyk, R. Rajimehr, S. M. Reader, P. R. Roelfsema, D. A. Rudko, M. F. S. Rushworth, B. E. Russ, J. Sallet, M. C. Schmid, C. M. Schwiedrzik, J. Seidlitz, J. Sein, A. Shmuel, E. L. Sullivan, L. Ungerleider, A. Thiele, O. S. Todorov, D. Tsao, Z. Wang, C. R. E. Wilson, E. Yacoub, F. Q. Ye, W. Zarco, Y.-D. Zhou, D. S. Margulies, C. E. Schroeder, An open resource for non-human primate imaging, *Neuron*, Vol. 100, No. 1, pp. 61-74, October, 2018.

[11] W. Chen, *Investigation on Automatic Segmentation of Macaque Brain Tissues and Anatomical Structures Based on 7T MR Images*, M. S. Thesis, Zhejiang University, Hangzhou, China, 2018.

[12] Y. Huo, Z. Xu, K. Aboud, P. Parvathaneni, S. Bao, C. Bermúdez, S. M. Resnick, L. E. Cutting, B. A. Landman, Spatially Localized Atlas Network Tiles Enables 3D Whole Brain Segmentation from Limited Data, *International Conference on Medical Image Computing and Computer-Assisted Intervention*, Granada, Spain, 2018, pp. 698-705.

[13] G. Zhao, F. Liu, J. A. Oler, M. E. Meyerand, N. H. Kalin, R. M. Birn, Bayesian convolutional neural network based MRI brain extraction on nonhuman primates, *Neuroimage*, Vol. 175, pp. 32-44, July, 2018.

[14] D. Zhang, Q. Guo, G. Wu, D. Shen, Sparse Patch-Based Label Fusion for Multi-Atlas Segmentation, *International Workshop on Multimodal Brain Image Analysis*, Nice, France, 2012, pp. 94-102.

[15] M. Yan, H. Liu, E. Song, Y. Qian, L. Jin, C.-C. Hung, Sparse patch-based representation with combined information of atlas for multi-atlas label fusion, *IET Image Processing*, Vol. 12, No. 8, pp. 1345-1353, August, 2018.

[16] M. Yan, H. Liu, X. Xu, E. Song, Y. Qian, N. Pan, R. Jin, L. Jin, S. Cheng, C.-C. Hung, An improved label fusion approach with sparse patch-based representation for MRI brain image segmentation, *International Journal of Imaging Systems and Technology*, Vol. 27, No. 1, pp. 23-32, March, 2017.

[17] R. Xia, Y. Ma, W. Wang, Y. Luo, M. Shang, Multi-atlas segmentation algorithm based on resampling, *Computer engineering and design*, Vol. 39, No. 8, pp. 2587-2592, August, 2018.

[18] Y. Liu, Y. Wei, C. Wang, Subcortical brain segmentation based on atlas registration and linearized kernel sparse representative classifier, *IEEE Access*, Vol. 7, pp. 31547-31557, March, 2019.

[19] J. A. Scott, D. Grayson, E. Fletcher, A. Lee, M. D. Bauman, C. M. Schumann, M. H. Buonocore, D. G. Amaral, Longitudinal analysis of the developing rhesus monkey brain using magnetic resonance imaging: birth to adulthood, *Brain Structure and Function*, Vol. 221, No. 5, pp. 2847-2871, June, 2016.

[20] S. Gouttard, M. Styner, S. C. Joshi, R. G. Smith, H. C. Hazlett, G. Gerig, Subcortical structure segmentation using probabilistic atlas priors, *SPIE Medical Imaging*, Vol. 6512, pp. 1-11, March, 2007.

[21] R. Wolz, P. Aljabar, D. Rueckert, R. A. Heckemann, A. Hammers, Segmentation of subcortical structures and the hippocampus in brain MRI using graph-cuts and subject-specific a-priori information, *Proceedings of the Sixth IEEE international conference on Symposium on Biomedical Imaging: From Nano to Macro (ISBI'09)*, Boston, Massachusetts, USA, 2009, pp. 470-473.

[22] D. Wu, T. Ma, C. Ceritoglu, Y. Li, J. Chotiyanonta, Z. Hou, J. Hsu, X. Xu, T. Brown, M. I. Miller, S. Mori, Resource atlases for multi-atlas brain segmentations with multiple ontology levels based on T1-weighted MRI, *Neuroimage*, Vol. 125, pp. 120-130, January, 2016.

Biographies

Hong Shi obtained the master's degree from Taiyuan Institute of machinery in 2002, and she has been an information system project manager in 2015. Her research interest includes big data intelligent analysis, computer network education, image processing.

Leiyi Gao obtained the B.E. degree in computer science and technology from Taiyuan University of Technology, Taiyuan, China, in 2022, and she is now a postgraduate student of Taiyuan University of Technology. Her research interest includes computer vision, brain science.

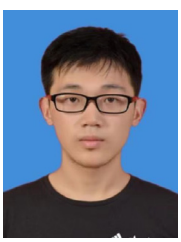

Ruixin Zhang obtained the B.E. degree in computer science and technology from Taiyuan University of Technology, Taiyuan, China, in 2022, and he is now a postgraduate student of Taiyuan University of Technology. His research interest includes image enhancement and image super-resolution.

Junzhu Wang obtained the B.E. degree from China University of Petroleum in 2019.Currently studying for a master's degree at Taiyuan University of Technology. His research interest includes low light image enhancement, image defogging.

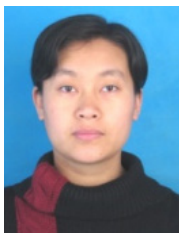

Hongxia Deng obtained the Ph.D. degree in computer application technology from Taiyuan University of Technology in 2013. And the same time she has been an associate professor. Her research interest includes computer vision, image processing, big data intelligent analysis, brain science.